ADVANCED OPTICAL MATERIALS
www.advopticalmat.de

$MCaH_xF_{3-x}$ (M = Rb, Cs): Synthesis, Structure, and Bright, Site-Sensitive Tunable Eu^{2+} Luminescence

*Alexander Mutschke, Thomas Wylezich, Atul D. Sontakke, Andries Meijerink, Markus Hoelzel, and Nathalie Kunkel**

Dedicated to Prof. H. P. Beck on the occasion of his 80th birthday

With increasing interest in mixed-anionic hydrides, a number of interesting properties have been reported. Here, the structural and optical properties of (Eu^{2+}-doped) $MCaH_3$–$MCaF_3$ (M = Rb, Cs) are investigated. For M = Rb, a complete hydride–fluoride solid solution series is found and for M = Cs, the known solid solution series ($0 \le x \le 1.70$) can be extended to $x = 3$. In case of Cs, a very bright luminescence emission is observed in Eu^{2+}-doped samples, whereas the luminescence is fairly weak in Rb based compounds. With increasing hydride content, a shift of the emission color from cyan-green to red can be observed. In contrast to earlier reports for mixed fluoride–hydride host, the redshift is not a gradual shift of a single broad emission band, but the appearance of new narrow emission bands on the low energy side, which are assigned to the occupation of sites with higher hydride content. Consequently, this finding represents the first example in a mixed anionic hydride with a site-sensitive emission for sites with locally varying hydride content in the first coordination sphere and may serve as a general example for emission color tuning taking advantage of mixed-anionic compounds.

1. Introduction

Due to the increasing interest in alternative energy storage, materials for hydrogen-based energy storage have been studied.[1–2] As a result of the similar radii of fluoride and hydride ions, structural similarities between metal hydrides and fluorides can be found[3] and fluoride substitution in metal hydrides is, for instance, proposed to tune the temperature of hydrogen release for thermal energy storage applications and thermally activated anion diffusion was studied.[4–6] Since tuning the anion chemistry is known to allow for a tailoring of the emission properties of the 5d–4f transition of Eu^{2+},[7–10] in the following, the structural and optical properties of the (Eu^{2+}-doped) systems $MCaH_3$–$MCaF_3$ (M = Rb, Cs) are investigated.

In case of M = Rb, so far no solid solution series was reported and the pure hydride and fluoride both crystallize in the ideal cubic perovskite structure type at room temperature.[11–15] For M = Cs, the partial solid solution series $CsCaH_xF_{3-x}$ ($0 \le x \le 1.70$) crystallizing in the cubic perovskite structure type has been reported earlier[16] as well as the pure hydride $CsCaH_3$.[17] However, due the synthesis route starting from CsF, CaF_2, and CaH_2, the possible composition range of the solid solution was limited to an upper limit of $x = 2$. In case of the lighter M = K, a solid-solution series with a miscibility gap as well as a change from a tetragonal structure with partial anion ordering to the $GdFeO_3$ structure type for fluoride rich samples has been reported.[18–19] Doped with rare earth ions and codoped with divalent manganese, alkali alkaline earth fluoroperovskites have been of interest for photoluminescence application and radiation dosimetry.[20–28] For instance, Sommerdijk and Bril reported on weak Eu^{2+} luminescence in $RbCaF_3$ (475 nm at 300 K) and bright green emission in $CsCaF_3$. Lately, Eu^{2+} emission has also been studied in such hydride–fluoride solid solution series or hydrides with fluoride structural analogs,

A. Mutschke, Dr. T. Wylezich, Dr. N. Kunkel
Chair for Inorganic Chemistry with Focus on Novel Materials
Technical University of Munich
Lichtenbergstr. 4, Garching 85748, Germany
E-mail: nathalie.kunkel@uni-goettingen.de

The ORCID identification number(s) for the author(s) of this article can be found under https://doi.org/10.1002/adom.202002052.

DOI: 10.1002/adom.202002052

Dr. T. Wylezich, Dr. N. Kunkel
Institut für Anorganische Chemie
Georg-August-University Goettingen
Tammannstr. 4, Goettingen 37077, Germany

Dr. T. Wylezich, Dr. N. Kunkel
Woehler Research Institute for Sustainable Chemistry (WISCh)
Georg-August-University Goettingen
Tammannstr. 2, Goettingen 37077, Germany

Dr. A. D. Sontakke, Prof. A. Meijerink
Condensed Matter & Interfaces
Debye Institute for Nanomaterials Science
Utrecht University
Princetonplein 1, Utrecht 3584 CC, The Netherlands

Dr. M. Hoelzel
Heinz Maier-Leibnitz-Zentrum (MLZ)
Technische Universität München
Lichtenbergstr. 1, Garching 85748, Germany

such as $MMgH_xF_{3-x}$ (M = Na, K, Rb), K_2MgH_4, $LiMH_3$ (M = Sr, Ba), $LiSr_2SiO_4H$ or $Sr_5(BO_3)_3H$,[29–36] and a correlation between the hydride content and redshift of the emission energies was found, which can be explained by the stronger nephelauxetic effect of hydride compared to fluoride.[37]

Here, we present the structural and optical properties of Eu^{2+}-doped samples of $MCaH_3$–$MCaF_3$ (M = Rb, Cs). In contrast to earlier reports on mixed hydride–fluorides, where a red shift of a single emission band could be observed with increasing hydride content, in the present case the changes in the emission color are rather caused by additional new emerging emission bands in the orange/red emission range. These new emissions bands exhibit narrow bandwidths and are assigned to a site-sensitive Eu^{2+} 5d–4f emission originating from different local F^-/H^- environments with different hydride content.

2. Results and Discussion

The undoped compounds $MCaH_xF_{3-x}$ (M = Rb, Cs) were obtained as colorless powders. On Eu^{2+} doping, the higher hydride content samples of $MCaH_xF_{3-x}$ (M = Rb, Cs) showed slightly red coloration. In the $CsCaH_3$ sample, the side phase Cs_2CaH_4 is always additionally found, which also had earlier been mistaken for $CsCaH_3$[38] and later it was clarified that both phases coexists.[17,39] While the Eu^{2+}-doped $RbCaH_xF_{3-x}$ did not show any strong emission even at liquid nitrogen temperature, bright cyan-green to red emission could be observed from $CsCaH_xF_{3-x}$ (see **Figure 1**).

2.1. Crystal Structure of $MCaH_xF_{3-x}$ (M = Rb, Cs)

Since the pure $MCaH_3$ (M = Rb, Cs) as well as $MCaF_3$ (M = Rb, Cs) crystallize in the ideal cubic perovskite structure in space group $Pm\bar{3}m$ (221), the solid solution series were found to crystallize isotypic as well. Here, only one distinct anion site (3c) is present which can be occupied by hydride or fluoride. Since no symmetry reduction could be noticed in the diffraction patterns, an ordered anion distribution, which would lead to a splitting of the 3c site, is ruled out. Additionally, Raman spectra were recorded (see Figures S1 and S2 in the Supporting Information) and no signals could be observed. This is consistent with the expectation that due to the Raman-inactive space group symmetry (O_h^1) of the ideal cubic perovskite structure no Raman signals are supposed to be visible. For example, however, for the tetragonal low temperature phase ($I4/mcm$,D_{4h}^{18}) of $RbCaF_3$ Raman signals are observed.[14]

Figure 1. Photographic images of the solid solution series $CsCaH_xF_{3-x}$:Eu^{2+} ($x \leq 2.5$) under day light (top) and the corresponding emission glow under 376 nm UV irradiation (bottom). (From left to right: x = 0, 0.25, 0.5, 0.75, 1.0, 1.5, 2.0, and 2.5.)

X-ray powder diffraction patterns were recorded and analyzed by the means of Rietveld refinement. Here, the total occupancy of the anion site (3c) by hydride and fluoride was set to 1, as it can be expected for an ionic compound. The fluoride content was refined and the remaining anion content assumed to be hydride. This was double-checked for several samples by analyzing the hydride content via elemental analysis (see the Experimental Section). Furthermore, for $CsCaD_{1.5}F_{1.5}$ also a neutron powder diffraction pattern was recorded and simultaneously refined together with the X-ray data. In contrast to X-ray data, where hydrogen is nearly invisible, ^2H has a bound coherent scattering length of 6.671(4) fm,[40] so that its position and occupation numbers can be reliably determined from neutron diffraction. Bound coherent scattering lengths for ^{19}F, ^{nat}Ca, and ^{133}Cs are 5.654(10), 4.70(2), and 5.42(2) fm, respectively.

The X-ray powder diffraction patterns obtained for the solid solution series $MCaH_xF_{3-x}$ (M = Rb, Cs) as well as the refined lattice parameters (a) as function of the hydrogen content x for both solid solution series are shown in **Figure 2**.

For both systems it can be clearly seen that with increasing hydride content, the Bragg reflections are gradually shifted toward smaller 2θ angles. This is in agreement with previous reports of hydride–fluoride solid solution series,[30] where the crystal lattice gradually expands with incorporation of hydride and can be explained by the higher thermal vibration of hydride due to its lower mass and the less polarizable character of fluoride. Furthermore, some reflections lose scattering intensity by the hydride–fluoride exchange. This is most noticeable on the Bragg reflection at ≈35° 2θ (111). While this reflection is strongly visible for the pure fluorides $RbCaF_3$ and $CsCaF_3$, its intensity gradually diminishes by increasing the hydride content, being barely visible for the pure hydrides $RbCaH_3$ and $CsCaH_3$. This is in good agreement with hydride incorporation, since as more fluoride ions are exchanged by hydrides, the scattering power of some lattice planes is reduced since hydride is a much weaker X-ray scatterer than fluoride. The cell parameters were refined using the program package FullProf. An exemplary refinement plot is depicted in the **Figure 3**a. Refined lattice parameters as well as interatomic distances and H-content of $RbCaH_xF_{3-x}$ are listed in Table S1 (Supporting Information), additional structural information in Tables S2 and S3 (Supporting Information).

As seen in Figure 2c a linear increase of the lattice parameter can be assumed, hence the following relation for the cell parameters and cell volume in dependency of the hydride

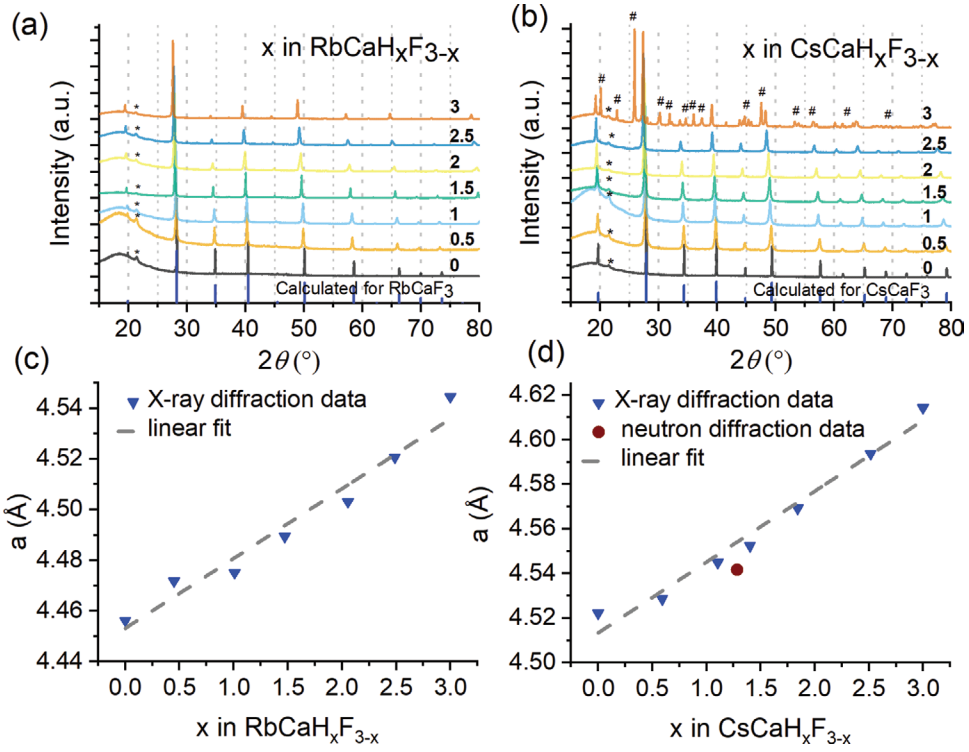

Figure 2. X-ray diffraction patterns of the solid solution series a) $RbCaH_xF_{3-x}$ and b) $CsCaH_xF_{3-x}$. The vertical dotted lines are meant to guide the eye. The asterisks mark a background reflection caused by the grease used to fixate the sample between the kapton foil. # marks reflection belonging to the side phase Cs_2CaH_4. Refined cell parameters (*a*) plotted in dependency of the hydride (*x*) content in the mixed phase c) $RbCaH_xF_{3-x}$ and d) $CsCaH_xF_{3-x}$.

content *x* can be formulated for the solid solution series $RbCaH_xF_{3-x}$

$$a = 0.028(3)x\text{Å} + 4.453(5)\text{Å} \quad (1)$$

$$V = 1.7(1)x\text{Å}^3 + 88.2(2)\text{Å}^3 \quad (2)$$

In case of the heavier homologues $CsCaH_3$ and $CsCaF_3$ a solid solution series $CsCaH_xF_{3-x}$ with an upper limit $x = 1.7$ had already been known.[16] Since only CsF and no elemental Cs or CsH had been used in the reported synthesis route, an upper limit of $x = 2.0$ was set due to the starting materials. To test if high hydride contents can be obtained, we used elemental cesium metal, which was hydrogenated during the reaction, and were able to synthesize the complete solution series $CsCaH_xF_{3-x}$.

However, the side phase Cs_2CaH_4 is clearly visible (marked with #) and unavoidable with the accessible synthesis methods. A Rietveld refinement plot thereof is depicted in Figure 3b.

To check for hydrogen positions and anion distribution, an additional neutron powder pattern was recorded for phase $CsCaD_{1.5}F_{1.5}$. The Rietveld refinement of the structure using the neutron data is depicted in Figure 3c. Refinement with a lower space group symmetry that allows for ordering of the anions (instead of a random distribution of F^- and H^- over the anion sites) was tested, but resulted in a strong deviation of the calculated refinement from the measured pattern. Hence, a statistical distribution of the anions in the ideal perovskite structure is assumed. As expected, the lattice parameter of the deuteride is slightly smaller than for the corresponding hydride, which is typical due to the higher mass and therefore lower thermal vibration of ^2H compared to ^1H.[41]

Refined lattice parameters as well as interatomic distances and H-content of the solid solution series $CsCaH_xF_{3-x}$ are listed in Table S4 (Supporting Information), additional information on the refinement can be found in Tables S5 and S6 (Supporting Information).

As can be seen in Figure 2d the lattice parameter *a* shows a nearly linear increase with increasing hydride content and the relation of *a* and cell volume *V* as a function of hydride content obtained from X-ray data can be formulated as follows

$$a = 0.032(2)x\text{Å} + 4.513(4)\text{Å} \quad (3)$$

$$V = 2.0(2)x\text{Å}^3 + 91.9(3)\text{Å}^3 \quad (4)$$

To further substantiate the incorporation of hydrogen within the crystal lattice and to confirm the values obtained from Rietveld refinement, elemental analysis of the hydrogen content of three mixed phases ($x = 0.5, 1.5, 2.5$) of both solid solution series has been carried out. The determined hydrogen content compared to the determined values obtained by Rietveld refinement is shown in Tables S7 and S8 (Supporting Information). All obtained values of the elemental analysis reports are depicted in Figures S4–S6 (Supporting Information).

The determined weight percentages by Rietveld refinement are very close to the values of the mixed phases with ideal

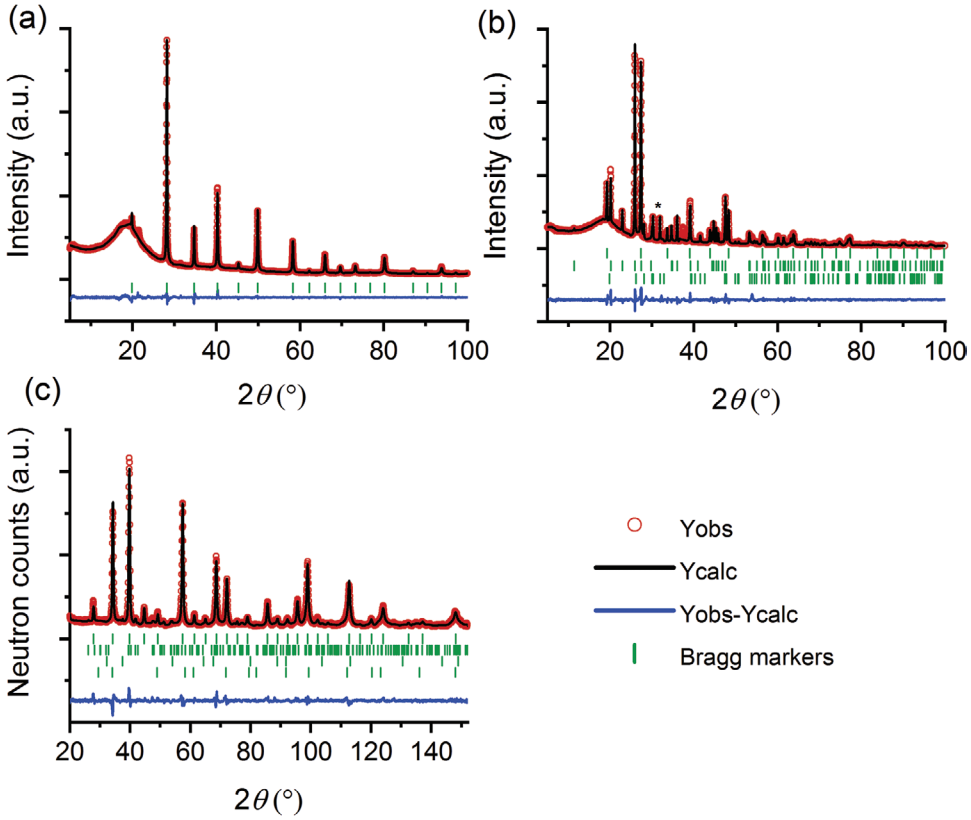

Figure 3. X-ray powder diffraction Rietveld refinement plots of a) the crystal structure of $RbCaHF_2$, and of b) the crystal structure of $CsCaH_3$. Bragg markers from top to bottom: $CsCaH_3$ (31.6(4) wt%), Cs_2CaH_4 (45.6(5) wt%), and CaH_2 (22.8(4) wt%). $R_p = 4.0\%$, $R_{wp} = 5.94$, $R_{exp} = 3.91$, $X^2 = 2.31$. The asterisk (*) marks a Bragg refection of an unidentified sidephase. It was excluded from Rietveld refinement. c) Rietveld refinement plot of the neutron diffraction pattern. Bragg markers from top to bottom: $CsCaD_{1.5}F_{1.5}$ (97.04 wt%), CaD_2, (2.15 wt%), CaO (0.43 wt%), CaF_2 (0.39 wt%). $R_p = 5.10\%$, $R_{wp} = 6.53\%$, $R_{Bragg} = 3.15\%$, $X^2 = 4.97$.

stoichiometric compositions. This finding could also be confirmed by elemental analysis, which shows a good agreement with the targeted compositions with only small deviations.

2.2. Luminescence Properties of Eu^{2+}-Doped $CsCaH_xF_{3-x}$

As shown in Figure 1, the solid solution series of $CsCaH_xF_{3-x}$ exhibit bright Eu^{2+} emission under UV excitation causing intense cyan-green to deep red emission glow. **Figure 4**a presents the corresponding luminescence spectra at room temperature. The bright cyan-green emission found in the fluoride $CsCaF_3$:Eu^{2+} was first described by Sommerdijk and Bril in 1975.[24] In a following publication, the authors also described a large redshift of the luminescence of 100 nm when decreasing the temperature from 300 to 77 K, which they explain by the existence of two distinct Eu^{2+} centers.[23] However, compared to other fluorides the Stokes shift is rather large; for instance, in $LiBaF_3$ or $KMgF_3$, Eu^{2+} 4f–4f emission could be observed due to the high-lying 5d states for Eu^{2+} on the large 12-coordinated lattice site in these fluoride perovskites.[42,43] The observation of longer wavelength emission in $CsCaF_3$ reflects that here Eu^{2+} substitutes on the six-coordinated Ca^{2+} site (see Figure S7 in the Supporting Information). Dorenbos ascribed the large Stokes shift and the comparatively wide emission band in $CsCaF_3$:Eu^{2+} to an anomalous Eu^{2+} luminescence.[28] Another explanation by Happek et al. assumed a Jahn–Teller distortion in the excited $5d^1$ state.[27]

As clearly seen in Figure 4a, the emission red shift with increasing hydride content as perceived with the naked eye is not solely caused by a red shift of a single emission band, but it involves a rather interesting phenomenon demonstrating appearance of narrowband emissions at lower energies and their subsequent intensity tuning. The emission of $CsCaF_3$ found here has an emission maximum of 510 nm and is same as the value found in earlier reports.[23,27–28] As the hydride content within the mixed phase increases, a small shift of the emission band of about 30 nm can be observed unto the phase $CsCaH_{0.5}F_{2.5}$, showing its emission maximum at ≈540 nm. The red shift agrees with earlier observations of other mixed hydride–fluorides and pure hydrides that all show a red shift caused by the nephelauxetic effect induced by the more polarizable and covalent hydride ions compared to fluoride.[29–37] However, emission spectra of the $CsCaH_xF_{3-x}$ solid solutions appear to exhibit several rather narrower emission bands, which become more prominent in samples with a hydride content above $x \geq 0.5$. The emission spectra show the emergence of emission bands at roughly 540, 575, 635 nm, etc. The emission band at 540 nm gradually loses intensity with further increasing hydride content in the solid solutions and shifts the emission maxima to newly emerged emission band at about 575 nm.

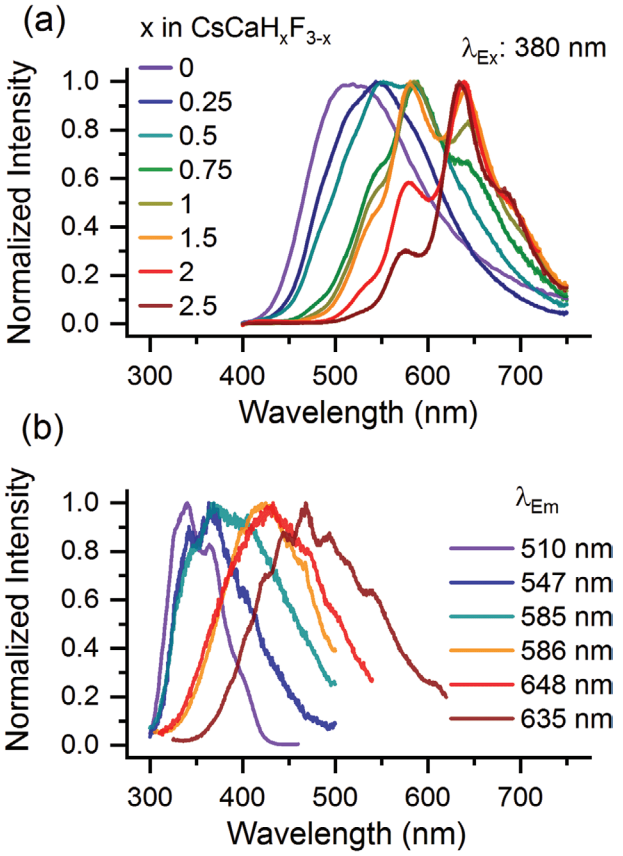

Figure 4. a) Room temperature PL spectra of the Eu^{2+} (1 mol% regarding Ca^{2+} via addition of EuF_2) doped solid solution series of $CsCaH_xF_{3-x}$; and b) the PLE spectra monitoring peak emission in different samples. The samples are identified with line colors as indicated in (a). λ_{exc} = 380 nm for PL in (a), whereas the PLE spectra were monitored at different wavelengths as indicated in (b).

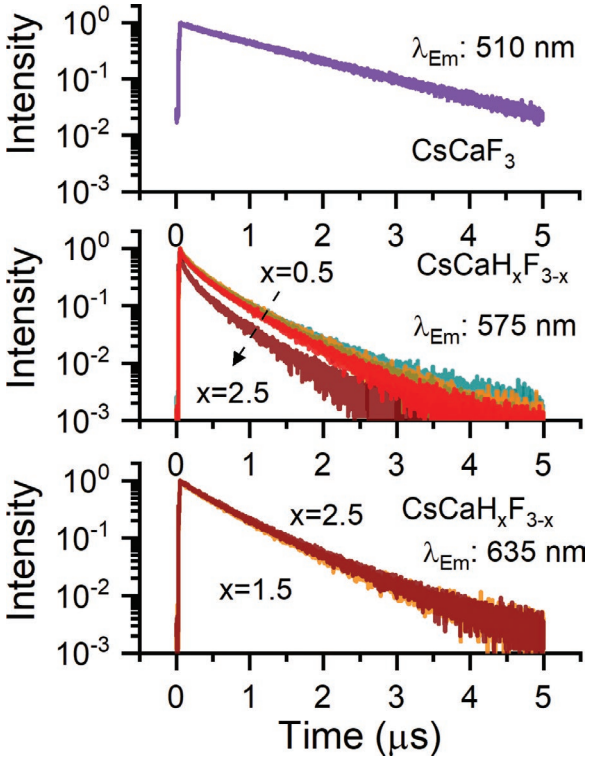

Figure 5. Eu^{2+} PL decay curves in $CsCaH_xF_{3-x}$ compounds monitored at different peak emission wavelengths. The excitation wavelength is 375 nm. Doping with Eu^{2+} via addition of EuF_2 during synthesis.

The 575 nm emission band also loses intensity for solid solutions with a hydride content $x > 1.5$, while the emission band at ≈635 nm reaches its intensity maximum with a hydride content of $x = 2$. Figure 4b presents the PLE spectra of different samples monitoring the respective peak emission wavelengths. The PLE spectra reveal structureless profiles, but consistently shifts toward longer wavelength following the emission wavelength shift and hydride contents. This suggests that the different emission bands are arising from different sites in $CsCaH_xF_{3-x}$ solid solution. A careful observation reveals that the excitation band monitoring same emission wavelength in different samples also differ. The higher hydride content composition exhibits relatively larger red shifted PLE.

The appearance of narrowband PL with hydride contents is rather unusual and may be caused by several effects. As in case of the pure fluoride, an excitonic emission might also be discussed. In rocksalt-type alkali metal halides as well as in alkaline-earth metal fluoride halides, different types of defects have been modeled and experimentally observed, such as self-trapped holes, electrons trapped at halide-vacancies or Schottky type lattice defects in BaFCl.[44–46] Given the hydride–fluoride analogy[5] and recent observations of defect formation in mixed anionic hydrides,[47] defect formation could be a possible explanation. However, this does not explain the narrower nature of emission bands. Furthermore, since Eu^{2+}-emission in pure CaH_2 was reported to be at 764 nm and exhibits significantly broadband profile (full width at half maximum, FWHM, ≈ 200 nm),[48] the possibility of a possible luminescent CaH_2:Eu^{2+} side phase can be ruled out. A more likely explanation might be the occupation of sites with different hydride content. For a statistical distribution, locally, different sites with different F:H ratio may appear, where such sites can exhibit relatively stronger site rigidity brought about by mixed anions offering a more compact packing of coordination sphere, and thus leading narrower emissions. With increasing overall hydride content, the weight fractions of the different arrangements will follow the relative F/H ratio, leading to an increase in lower energy emission sites with hydrogen rich arrangement over the fluorine rich arrangements. Analysis of low temperature emission spectra (vide infra) support this explanation.

Figure 5 presents the Eu^{2+} PL decay curves for different emission peaks in $CsCaH_xF_{3-x}$ solid solutions. The $CsCaF_3$:Eu^{2+} sample reveals single exponential decay profile, agreeing well with single Eu^{2+} site in this compound.[49] With hydride inclusion, the prominent narrowband emissions appear at around 575 and 635 nm. The decay curves monitoring at 575 nm reveals nonexponential feature, and exhibits faster relaxation for higher hydride contents, whereas the 635 nm decay curves did not show significant variation with hydride contents. This suggests that for the 575 nm emission an additional decay path opens which increases as hydride contents increase. The results are consistent with PL observations. Accordingly, with increasing

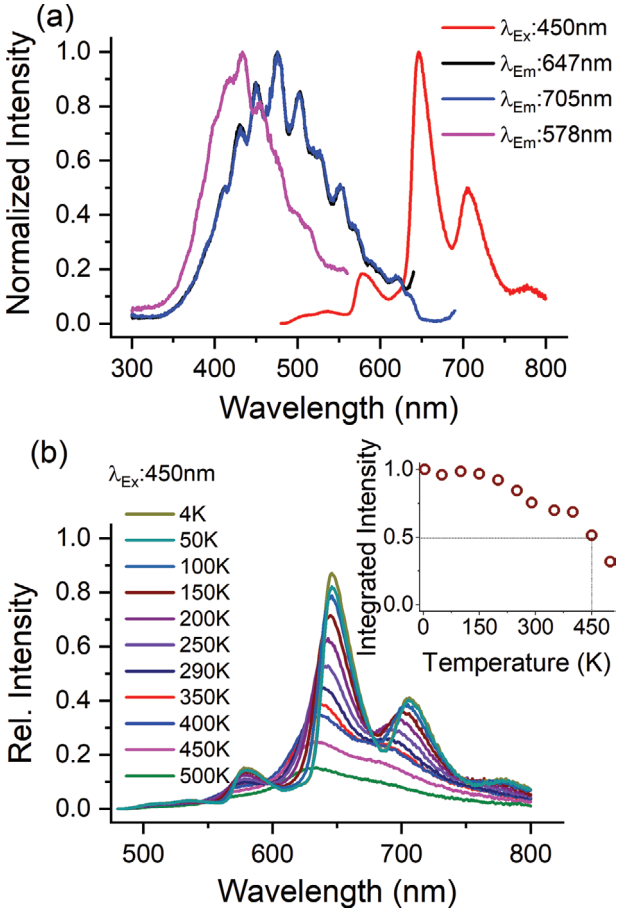

Figure 6. a) 4.2 K PL–PLE spectra of $CsCaH_2F:Eu^{2+}$ sample; and b) temperature dependence of PL. The inset shows a plot of integrated intensity versus temperature. The sample was doped with Eu^{2+} by the addition of EuF_2 during synthesis.

hydride contents in $CsCaH_xF_{3-x}$, the fraction of longer wavelength emitting sites increases which additionally quenches the 575 nm emission following resonant energy transfer from the 575 nm sites to the red emitting sites.[50]

To get further insight on Eu^{2+} luminescence in $CsCaH_xF_{3-x}$ solid solution, the luminescence properties were investigated at 4.2 K. **Figure 6**a presents the PL and PLE of $CsCaH_2F:Eu^{2+}$ (1%) sample at 4.2 K. The PL bands are better resolved and can be distinctively identified. Accordingly, there are four prominent emissions peaking at 578, 647, 705, and 780 nm. In addition, few weak emission bands could be identified at around 510 and 540 nm. The PLE monitored for 578 nm emission peaks at 427 nm, whereas for 647 and 705 nm, the PLE is almost identical with peak maximum at about 470 nm. This indicates that the 705 nm emission is primarily fed through sensitization from 647 nm emitting Eu^{2+} ions. This suggests that the 705 nm emitting sites are less abundant than the 647 and 578 nm emitting sites. Also, a clear evidence of multiple sites is evident from the differences in PLE of 578 nm emission and the PLE of the 647 and 705 nm emission.

A tentative assignment can be made to the different narrow emission peaks to Eu^{2+} with 0 to 6 H^- (and thus 6–0 F^-) in the first octahedral coordination shell. Based on the observed peak intensities and the relative intensities expected based on a statistical occurrence of a specific 6-coordination in $CsCaH_2F$ (66.6% H^-, 33.3%F^-), the weak 510 nm emission feature is assigned to Eu^{2+} with 0 or 1 H^- (expected abundances 0.1% and 1.6%). The 540 nm peak to Eu^{2+} with a 2 $H^-/4F^-$ coordination (8.2%), 578 nm to Eu^{2+} with $3H^-/3F^-$ (21.9%), 647 nm to $4H^-/2F^-$ (32.9%, most abundant coordination), 705 nm to $5H^-/1F^-$ (26.3%), and 780 nm to Eu^{2+} with full octahedral H^- coordination (8.8%). There is a good agreement with the observed relative intensities and expected intensities based on a statistical distribution of F^- and H^- in the first coordination shell. For $CsCaH_2F$ indeed the $4H^-/2F^-$ coordination is the most abundant in line with the observation of the strongest emission line at 647 nm. Energy transfer between the different Eu^{2+} sites can explain some of the observed differences such as the somewhat lower than expected relative intensity of the 578 nm emission line due to energy transfer to Eu^{2+} ions emitting at 647 nm, in line with the faster decay observed for the 575 nm emission (see Figure 5). It is interesting to see that with every additional H^- replacing F^- the emission band shifts to ≈1500 cm^{-1} lower energies, although there some variation in the energy shifts. It will be interesting to use recently developed model for energy level calculations for the $4f^65d$ state of Eu^{2+} to verify the observed energy shifts upon gradually changing the coordination from $[EuF_6]^{4-}$ to $[EuH_6]^{4-}$.[51] Possibly, the observation of multiple site emission instead of a broad band might be caused by the occupation of the octahedral Ca^{2+}-site, which might, with its smaller ionic radius lead to a rather rigid environment. In previously studied perovskite hydride, Eu^{2+} luminescence was never reported for a Ca^{2+}-containing perovskite. The emission spectra as a function of temperature are presented in Figure 6b. The spectra show a small peak blueshift and band broadening with temperature. A blueshift in the emission of Eu^{2+} or Ce^{3+} with increasing temperature may have several reasons, among others the increase of the activator–ligand distance and the consequent decrease of the crystal field strength and covalency of the ligand-activator bond.[27,52] The observed blueshift of the main emission maximum from Figure 6b (see Figure S8 in the Supporting Information) is ≈370 cm^{-1}, larger than thermochromic blueshifts of the $4f^65d^1$–$4f^7$ emission of Eu^{2+} in other halide hosts, but still significantly smaller than the blueshifts reported for pure borohydride systems.[52,53]

The FWHM for the most prominent emission at 647 nm is about 28 nm at 4.2 K and increases till 35 nm at 300 K with the peak position shifting from 647 to 635 nm. This is due to temperature-induced effects, such as site expansion, which leads to a reduced crystal field strength, and an increase in bond length variations. The integrated PL intensity is constant till 150 K and then slowly reduces. The $T_{50\%}$ is at about 450 K, suggesting good PL stability of studied mixed halide-fluorides. It is difficult to evaluate individual thermal stability of different bands due to their intermixed nature, both in PL and PLE features as well as thermally induced spectral changes and temperature dependent energy transfer between different Eu^{2+} sites. Nevertheless, it is evident that the emission is fairly stable till room temperature and all emission bands are present even at room temperature spectrum.

Figure 7a shows the Eu^{2+} PL in $CsCaH_2F$ compounds having different doping concentrations. Interestingly, the low

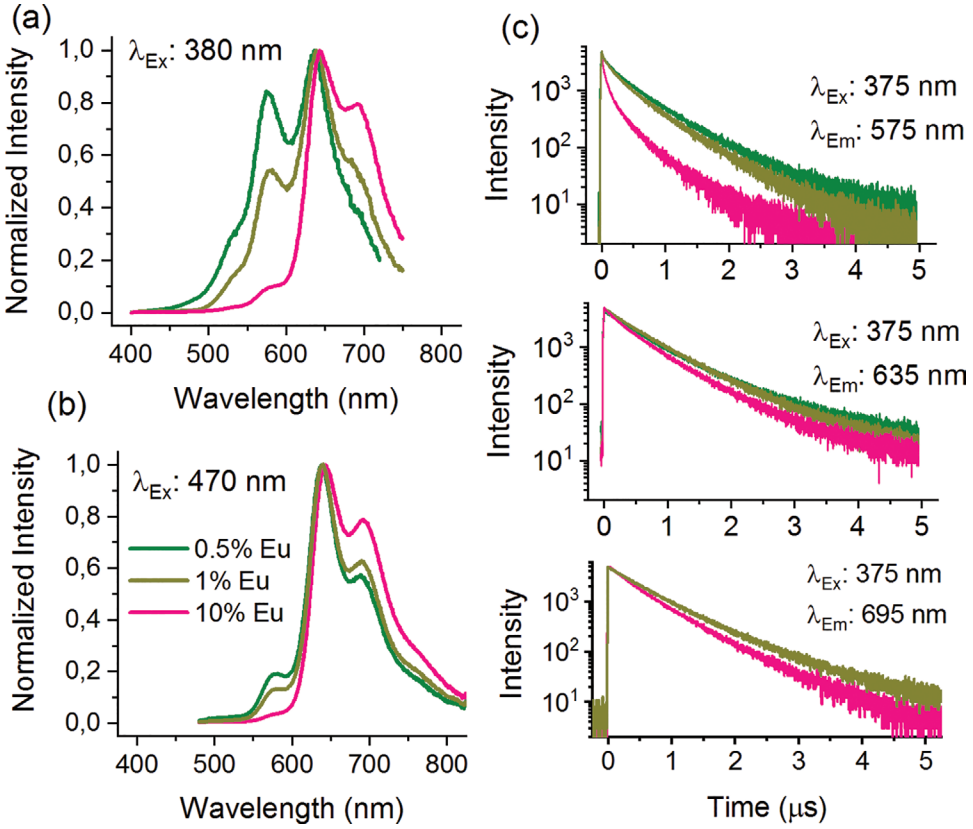

Figure 7. PL spectra of $CsCaH_2F$ doped with different Eu contents under a) 380 nm excitation and b) 470 nm excitation. The PL decay curves monitoring different emission peaks are presented in (c). The samples were doped with Eu^{2+} by adding the appropriate amounts of EuF_2 during synthesis.

Eu^{2+} concentration sample exhibits more prominent higher energy emission bands, which systematically decrease in intensity as the doping concentration increases. This is consistent with the energy transfer-based quenching. Similar effects are observed under 470 nm excitation (Figure 7b). The decay curves (Figure 7c) further confirm the energy transfer quenching as the 575 nm emission is quenched faster with increase in Eu^{2+} contents as demonstrated by the faster decay in the higher doped materials.

The observed redshift upon substitution of F^- by H^- is very interesting and offers great emission tunability. Both composition and doping concentration in $CsCaH_xF_{3-x}$ solid solution can easily be exploited to tune the emission color. In former case, the composition modification avails new sites with longer wavelength emissions, whereas in latter case, the higher doping increases population of emitting ions, thus increasing interionic interactions and promoting energy transfer to Eu^{2+} sites emitting at longer wavelength. The combined control over site distribution and energy transfer leads to unique capabilities to tune the emission color from green to deep red. It is also anticipated that the doping precursor may affect the dopant site distribution. To see the effect of dopant precursor, we prepared $CsCaH_2F:Eu^{2+}$ (1 mol%) sample using $CaH_2:Eu^{2+}$ as doping precursors ($CaH_2:Eu^{2+}$ where calcium and europium had been melted and the resulting alloy hydrogenated). **Figure 8**a presents the PL spectrum of $CsCaH_2F$ compounds doped using $CaH_2:Eu^{2+}$ and compared with the PL spectra of $CsCaH_2F$ compounds doped with 1% and 10% Eu using EuF_2 based precursor. Accordingly, the 575 nm emission band is totally quenched in 1% Eu^{2+} doped sample using $CaH_2:Eu^{2+}$ compared to the fluoride precursor sample. The spectrum matches more with 10% Eu^{2+} fluoride precursor doped sample at higher energy side but exhibits relatively brighter red emission and narrower emission profile. This is explained by the fact that the $CaH_2:Eu^{2+}$ based doping allows more Eu^{2+} ions in hydride rich sites, but as the overall Eu^{2+} concentration is less, the energy transfer is limited. The PLE spectrum reveals that the $CaH_2:Eu^{2+}$ doping offers Eu^{2+} in more covalent sites and energy transfer-based feeding is limited. A further confirmation of restricted energy transfer is witnessed from the PL decay curves (Figure 8b). Here, the 575 nm emission decay is relatively slower in $CaH_2:Eu^{2+}$ doped sample compared to similar spectral shape 10% EuF_2 doped sample. Moreover, the red emission at 635 nm PL decay is also less quenched in sample using $CaH_2:Eu^{2+}$ as precursor.

It is evident that the use of the $CaH_2:Eu^{2+}$ europium source leads to a higher probability of finding Eu^{2+} in a hydrogen rich arrangement. In contrast, the redshift of the emission with increasing europium concentration is assigned to energy transfer related quenching of higher energy emission bands which will lead to a preferential emission from the hydride-rich lower energy emission sites. The results are highly advantageous in spectral tuning and achieving narrowband emission

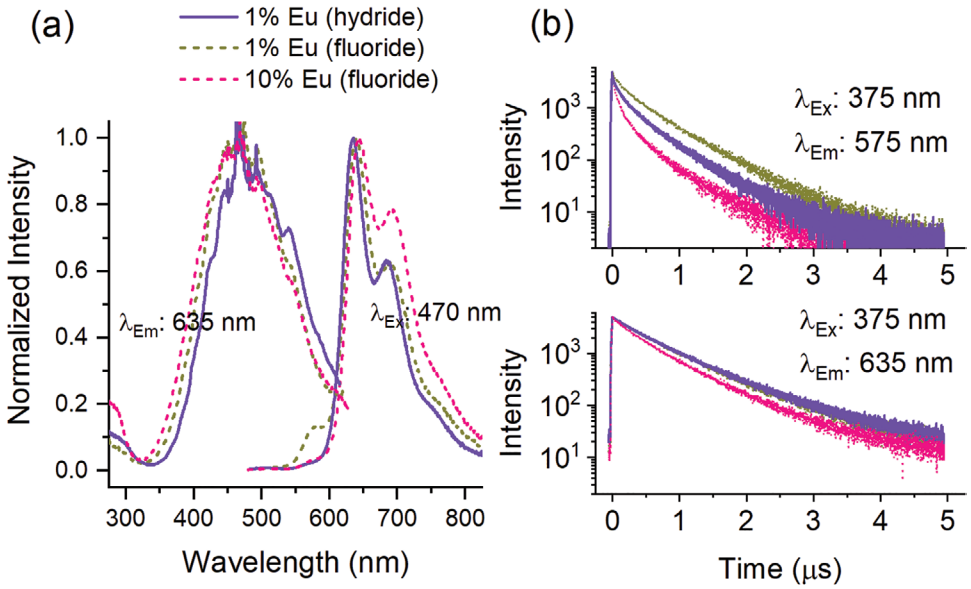

Figure 8. a) PL–PLE spectra of $CsCaH_2F:Eu^{2+}$ using $CaH_2:Eu^{2+}$ and EuF_2 as doping precursors; and b) respective decay curves monitoring different emission wavelengths.

in such mixed anionic hosts. The emission bandwidth of individual bands is as low as 30–40 nm at room temperature, which is relatively narrow and comparable to the emission bandwidth found in the green narrow-band emitter $RbLi(Li_3SiO_4)_2:Eu^{2+}$ (RLSO:Eu^{2+})[54] and the recently developed narrowband red emitting oxide nitride $Sr[Li_2Al_2O_2N_2]:Eu^{2+}$ (SALON:Eu^{2+}) phosphors.[55]

3. Conclusion

In the present work, we report the successful synthesis of the complete solid solution series $RbCaH_xF_{3-x}$ and $CsCaH_xF_{3-x}$ and find a bright Eu^{2+}-luminescence for M = Cs. In contrast to earlier reports on doped hydride materials, we did not observe a gradual redshift of a single broad band with increasing hydride content, but instead a step-wise color shift from cyan-green to red is observed. Replacing F^- by H^- reveals the appearance of several new relatively narrow emission bands on the lower energy side, which are explained by the change in F^-/H^- coordination for Eu^{2+} on the octahedral site in $CsCaH_xF_{3-x}$ from $[EuF_6]^{4-}$ to $[EuH_6]^{4-}$ with all possible intermediates and follows the overall F/H ratio in the samples. With regard to the increasing importance of mixed-anionic hydrides, these results are of interest for the design of phosphors using more stable mixed-anionic hydrides, for instance among the oxide, silicate or borate hydrides and can also deliver useful information about effects of varying hydride contents in a local environment.

4. Experimental Section

Synthesis: As the hydrides are sensitive to air and moisture and the fluorides are hygroscopic, all manipulations were carried out in an argon-filled glove box. To remove any traces of moisture, the binary fluorides were dried under dynamic vacuum at 200 °C for 2 h before use. The perovskites $MCaH_xF_{3-x}$ (M = Rb, Cs) can be synthesized from stoichiometric amounts of the alkaline metals with binary hydrides or fluorides. Therefor rubidium metal (Rb, 99.8%, Alfa Aesar) or cesium metal (Cs, 99.9%, Chempur) is grinded thoroughly in an agate mortar with the required amounts of rubidium fluoride (RbF, 99.9%, abcr) or cesium fluoride (99.99%, Chempur) and calcium hydride (CaH_2, prepared by hydrogenation of calcium ingots, Alfa Aesar, 99.5%) or calcium fluoride (99.95%, Alfa Aesar). These mixtures were heated in an autoclave made of a hydrogen-resistant alloy (Inconel Böhler 718) at 550 °C under 50 bars of hydrogen pressure (H_2, 99.9%, Westfalen AG) for ≈2 days. For $CsCaH_xF_{3-x}$ and $x \geq 2$ the reaction mixture was heated at 600 °C for 2 days to avoid the formation of Cs_2CaH_4 as a side product. The pure fluorides $MCaF_3$ (M = Rb, Cs) were synthesized from the solid-state reaction of the binary fluorides in arc welded Ni alloy ampules (Alloy 400, Eugen-Geyer GmbH). The ampules were enclosed in evacuated (≈10^{-2} mbar) quartz glass to avoid oxidation and decomposition of the ampule material. The reaction mixture was subsequently heated to 800 °C for 12 h. Doping with europium was achieved by adding either 1 mol% europium hydride (EuH_2, prepared by hydrogenation of europium metal, Eu, Alfa Aesar, 99.9%), 1 mol% europium fluoride (EuF_2, 99.9% Alfa Aesar) or $CaH_2:Eu^{2+}$ (prepared from the hydrogenation of Ca:Eu alloy) to the reaction mixtures. For neutron powder diffraction ≈4 g of $CsCaD_{1.5}F_{1.5}$ was synthesized as described above, using deuterium gas (D_2, 99.9%, AirLiquide) instead of hydrogen gas and CaD_2.

Characterization—X-Ray and Neutron Powder Diffraction: X-ray powder diffraction data were recorded on a Stoe STADI-P in transmission geometry with Cu-Kα_1 radiation (λ = 1.54056 Å), a curved Ge-monochromator (111) and a Dectris Mythen DCS 1K solid-state detector. In order to avoid decomposition of the samples during measurements, the powders were mixed with grease (glisseal HV, Borer Chemie) and placed between two kapton foils in a flat sample holder. Scattering angle corrections were determined by an external silicon standard (NIST SRM 640c). Neutron powder diffraction data of $CsCaD_{1.5}F_{1.5}$ were recorded at the high-resolution neutron powder diffractometer SPODI at the research reactor FRM II.[56] The sample was placed in a thin-walled 13 mm diameter vanadium cylinder sealed with an indium wire and a filling height of ≈4 cm. For the measurement the cylinder was placed inside a sample changer with a rotary engine. The diffractometer was operated in standard high-resolution mode in Debye–Scherrer geometry. As the monochromator, germanium (551) was used with a resulting wavelength of 1.548 Å and

a take-off angle of 155°. Data was collected with a multidetector system consisting of 80 ^{3}He detector tubes. By stepwise positioning of the detector array $\Delta 2\theta = 0.05°$, corresponding in 40 individual steps, the powder diffraction pattern in the range $0° \leq 2\theta \leq 160°$ was obtained after 4 h. LaB_6 was measured for ≈30 min as an external standard for angle correction. Crystal structure refinement was carried out using the program package FullProf with the Rietveld method.[57–57] Wavelength corrections were determined using the externally measured silicon standard (NIST SRM 640c). For profile fitting pseudo-Voigt functions were used. Zero shift, cell parameters, form factors, 4 asymmetry parameters, atomic parameters deuterium/hydrogen and fluorine content and thermal displacement parameters were refined. The background correction was carried out with linear interpolations of background points. In the case of $CsCaD_{1.5}F_{1.5}$ a joint Rietveld refinement of both X-ray and neutron data was carried out. Cell parameters were allowed to differ, while atomic parameters and occupations were coupled.

Characterization—Luminescence Spectroscopy: Luminescence emission and excitation spectra were recorded both on a Horiba Jobin Yvon Fluorolog 3 as well as a FLS920 spectrofluorometer from Edinburgh Instruments. In both cases, as excitation source, a 450 W Xe-lamp was used and for detection a R928 Hamamatsu photomultiplier tube was used. For the excitation beam, a double monochromator according to Czerny–Turner with 300 nm blaze (FLS920) or 330 nm blaze (Fluorolog) was used. For emission, a double monochromator (500 nm blaze) was used on the Fluorolog 3 and a single monochromator (500 nm blaze) on the FLS920. All spectra were corrected for lamp intensity and detector response. Decay measurements were recorded on the FLS920 spectrofluorometer with a pulsed diode laser (376.8 nm, Edinburgh Instruments) as excitation source and a Hamamatsu H74220 60 photomultiplier tube for detection. For cryogenic (4.2 K) measurements, the samples were cooled down using an Oxford Instruments liquid He flow cryostat. For temperature dependence study, liquid He flow cryostat attached with an Oxford instruments temperature controller was employed at 4.2–500 K temperature range.

Characterization—Elemental Analysis: Elemental analysis was conducted on a Vario El microanalyzer. Due to the samples being sensitive to air and moisture, ≈3 mg of the sample was packed within a small tin boat and folded several times to be sealed airtight before being analyzed. Then, they were heated under oxygen and the evolving hydride was analyzed quantitatively using a thermal conductivity detector. The measurements were each repeated twice.

Characterization—Raman Spectroscopy: Raman spectra were recorded on powders sealed in glass capillaries (0.3 mm diameter) on a Renishaw inVia Reflex Raman System equipped with a CCD detector and a $\lambda = 532$ nm laser in the range of 100–1000 cm^{-1}.

Further details of the crystal structure investigation(s) may be obtained from the Fachinformationszentrum Karlsruhe, 76344 Eggenstein-Leopoldshafen (Germany), on quoting the depository number CSD 2040237, CSD 2040629, CSD 2040630, CSD 2040682, CSD 2040714, CSD 2040715, CSD 2040716.

Supporting Information

Supporting Information is available from the Wiley Online Library or from the author.

Acknowledgements

The authors would like to thank the Research Neutron Source Heinz Maier-Leibnitz (FRM II) for beamline time. N.K. and T.W. thank the Fonds der Chemischen Industrie for a Liebig and a doctoral fellowship (Li 197/02) and Prof. Thomas Fässler for support. The authors thank Johanna Haimerl for help with synthetic work. The research leading to these results had received funding from the DFG (KU 3427/4-1, INST 186/1328-1, INST 186/1346-1) and the ATUMS Alberta/Technical University of Munich International Graduate School "Functional Hybrid Materials" (IRTG 2022; 245845833).

Open access funding enabled and organized by Projekt DEAL.

Conflict of Interest

The authors declare no conflict of interest.

Data Availability Statement

Research data are not shared.

Keywords

Eu^{2+} luminescence, hydride fluoride, perovskites, site-sensitivity

Received: November 30, 2020
Revised: January 4, 2021
Published online: February 4, 2021

[1] M. Hirscher, V. A. Yartys, M. Baricco, J. Bellosta von Colbe, D. Blanchard, R. C. Bowman, D. P. Broom, C. E. Buckley, F. Chang, P. Chen, Y. W. Cho, J.-C. Crivello, F. Cuevas, W. I. F. David, P. E. de Jongh, R. V. Denys, M. Dornheim, M. Felderhoff, Y. Filinchuk, G. E. Froudakis, D. M. Grant, E. M. Gray, B. C. Hauback, T. He, T. D. Humphries, T. R. Jensen, S. Kim, Y. Kojima, M. Latroche, H.-W. Li, M. V. Lototskyy, J. W. Makepeace, K. T. Møller, L. Naheed, P. Ngene, D. Noréus, M. M. Nygård, S.-i. Orimo, M. Paskevicius, L. Pasquini, D. B. Ravnsbæk, M. Veronica Sofianos, T. J. Udovic, T. Vegge, G. S. Walker, C. J. Webb, C. Weidenthaler, C. Zlotea, *J. Alloys Compd.* **2020**, *827*, 153548.
[2] M. Paskevicius, L. H. Jepsen, P. Schouwink, R. Černý, D. B. Ravnsbæk, Y. Filinchuk, M. Dornheim, F. Besenbacher, T. R. Jensen, *Chem. Soc. Rev.* **2017**, *46*, 1565.
[3] A. J. Maeland, W. D. Lahar, *Z. Phys. Chem.* **1993**, *179*, 181.
[4] T. D. Humphries, D. A. Sheppard, M. R. Rowles, M. V. Sofianos, C. E. Buckley, *J. Mater. Chem. A* **2016**, *4*, 12170.
[5] M. Heere, M. H. Sørby, C. Pistidda, M. Dornheim, B. C. Hauback, *Int. J. Hydrogen Energy* **2016**, *41*, 13101.
[6] D. Wiedemann, E. M. Heppke, A. Franz, *Eur. J. Inorg. Chem.* **2015**, 5085.
[7] M. Zeuner, S. Pagano, W. Schnick, *Angew. Chem., Int. Ed.* **2011**, *50*, 7754.
[8] P. Pust, V. Weiler, C. Hecht, A. Tücks, A. S. Wochnik, A.-K. Henß, D. Wiechert, C. Scheu, P. J. Schmidt, W. Schnick, *Nat. Mater.* **2014**, *13*, 891.
[9] G. J. Hoerder, S. Peschke, K. Wurst, M. Seibald, D. Baumann, I. Stoll, H. Huppertz, *Inorg. Chem.* **2019**, *58*, 12146.
[10] K. Horky, W. Schnick, *Chem. Mater.* **2017**, *29*, 4590.
[11] H. Wu, W. Zhou, T. J. Volovic, J. J. Rush, T. Yildirim, *Phys. Chem. C* **2009**, *113*, 15091.
[12] P. Vajeeston, P. Ravindran, H. Fjellvåg, *J. Chem. Phys.* **2010**, *132*, 114504.
[13] F. A. Modine, E. Sonde, W. P. Unruh, *Phys. Rev. B* **1974**, *10*, 1623.
[14] P.h. Daniel, M. Rousseau, J. Toulouse, *Phys. Rev. B* **1997**, *55*, 6222.
[15] K. S. Knight, *J. Solid State Chem.* **2018**, *263*, 172.
[16] H.-H. Park, J. Senegas, J. M. Reau, M. Pezat, B. Darriet, P. Hagenmuller, *Mater. Res. Bull.* **1988**, *23*, 1127.
[17] F. Gingl, T. Vogt, E. Akiba, K. Yvon, *J. Alloys Compd.* **1999**, *282*, 125.

[18] J.-P. Soulié, J.-P. Laval, A. Bouamrane, *Solid State Sci.* **2003**, *5*, 273.
[19] C. Pflug, H. Kohlmann, *Z. Anorg. Allg. Chem.* **2020**, *646*, 175.
[20] D. J. Daniel, A. Raja, V. Madhussodanan, O. Annalakshmi, P. Ramasamy, *Opt. Mater.* **2016**, *58*, 497.
[21] A. Raja, G. Annadurai, D. J. Daniel, P. Ramasamy, *J. Alloys Compd.* **2016**, *683*, 654.
[22] A. Raja, R. Nagaraj, K. Ramacandran, V. Sivasubramani, G. Amadurai, D. J. Daniel, P. Ramasamy, *Adv. Powder Technol.* **2020**, *31*, 2597.
[23] J. L. Sommerdijk, A. Bril, *J. Lumin.* **1976**, *11*, 363.
[24] J. L. Sommerdijk, A. Bril, *J. Lumin.* **1975**, *10*, 145.
[25] C. Gaedtke, G. V. Williams, S. Janssens, S. Raymond, D. Clark, *Radiat. Meas.* **2013**, *56*, 187.
[26] J. Garcia, M. W. A. Sibley, *J. Lumin.* **1988**, *42*, 109.
[27] U. Happek, M. Aycibin, A. M. Srivastava, H. A. Comanzo, S. Camardello, *ECS Trans.* **2009**, *25*, 39.
[28] P. Dorenbos, *J. Phys.: Condens. Matter* **2003**, *15*, 2245.
[29] C. Pflug, A. Franz, H. Kohlmann, *J. Solid State Chem.* **2018**, *258*, 391.
[30] T. Wylezich, S. Welinski, M. Hölzel, P. Goldner, N. Kunkel, *J. Mater. Chem. C* **2018**, *6*, 13006.
[31] J. Ueda, T. Wylezich, N. Kunkel, S. Tanabe, *J. Mater. Chem. C* **2020**, *8*, 5124.
[32] N. Kunkel, A. Meijerink, H. Kohlmann, *Phys. Chem. Chem. Phys.* **2014**, *16*, 4807.
[33] F. Gehlhaar, R. Finger, N. Zapp, M. Bertmer, H. Kohlmann, *Inorg. Chem.* **2018**, *57*, 11851.
[34] T. Wu, A. Ishikawa, T. Honda, H. Tamatsukuri, K. Ikeda, T. Otomo, S. Matsuishi, *RSC Adv.* **2019**, *9*, 5282.
[35] T. Wylezich, R. Valois, M. Suta, A. Mutschke, C. Ritter, A. Meijerink, A. J. Karttunen, N. Kunkel, *Chem. - Eur. J.* **2020**, *26*, 11742.
[36] N. Kunkel, T. Wylezich, *Z. Anorg. Allg. Chem.* **2019**, *645*, 137.
[37] H. Daicho, Y. Shinomiya, K. Enamoto, A. Nakano, H. Sawa, S. Matsuishi, H. Hosono, *Chem. Commun.* **2018**, *54*, 884.
[38] H. H. Park, M. Pezat, B. Darriet, *Rev. Chim. Miner.* **1986**, *23*, 323.
[39] W. Bronger, L. Breil, *Z. Anorg. Allg. Chem.* **1997**, *623*, 119.
[40] V. F. Sears, *Neutron News* **1992**, *3*, 26.
[41] V. P. Ting, P. F. Henry, H. Kohlmann, C. C. Wilson, M. T. Weller, *Phys. Chem. Chem. Phys.* **2010**, *12*, 2083.
[42] A. Meijerink, *J. Lumin.* **1993**, *55*, 125.
[43] N. S. Altsuler, L.-D. Livanova, A. L. Stolov, *Opt. Spectrosc.* **1974**, *36*, 72.
[44] K. Somaiah, H. Hari Babu, *Phys. Status Solidi B* **1983**, *117*, 75.
[45] R. C. Baetzold, *Phys. Rev. B* **1987**, *36*, 9182.
[46] R. C. Baetzold, K. S. Song, *Phys. Rev. B* **1993**, *48*, 14907.
[47] K. Hayashi, H. Hosono, *Phys. Chem. Chem. Phys.* **2016**, *18*, 8186.
[48] N. Kunkel, H. Kohlmann, A. Sayede, M. Springborg, *Inorg. Chem.* **2011**, *50*, 5873.
[49] S. M. Poort, A. Meyerink, G. Blasse, *J. Phys. Chem. Solids* **1997**, *58*, 1451.
[50] A. D. Sontakke, J.-M. Mouesc, V. Castaing, A. Ferrier, M. Salaün, I. Gautier- Luneau, V. Maurel, A. Ibanez, B. Viana, *Phys. Chem. Chem. Phys.* **2018**, *20*, 23294.
[51] J. Joos, P. F. Smet, L. Seijo, Z. Barandiaran, *Inorg. Chem. Front.* **2020**, *7*, 871.
[52] T. Wylezich, A. D. Sontakke, V. Castaing, M. Suta, B. Viana, A. Meijerink, N. Kunkel, *Chem. Mater.* **2019**, *31*, 8957.
[53] M. Suta, C. Wickleder, *J. Mater. Chem. C* **2015**, *3*, 5233.
[54] M. Zhao, H. Liao, L. Ning, Q. Zhang, Q. Liu, Z. Xia, *Adv. Mater.* **2018**, *30*, 1802489.
[55] J. Hoerder, M. Seibald, D. Baumann, T. Schröder, S. Peschke, P. C. Schmid, T. Tyborski, P. Pust, I. Stoll, M. Bergler, C. Patzig, S. Reißaus, M. Krause, L. Berthold, T. Höche, D. Johrendt, H. Huppertz, *Nat. Commun.* **2019**, *10*, 1824.
[56] M. Hoelzel, A. Senyshyn, N. Juenke, H. Boysen, W. Schmahland, H. Fuess, *Nucl. Instrum. Methods Phys. Res., Sect. A* **2012**, *667*, 32.
[57] J. Rodriguez-Carvajal, *Phys. Rev. B: Condens. Matter Mater. Phys.* **1993**, *192*, 55.
[58] H. M. Rietveld, *J. Appl. Crystallogr.* **1969**, *2*, 65.